scientific reports

Check for updates

OPEN

Preparation of $Ti_3C_2T_x$ modified rare earth doped PbO_2 electrodes for efficient removal of sulfamethoxazole

Dancheng Zhu, Yifan Wu, Kai Zheng, Hao Xu, Chao Chen, Jun Qiao & Chao Shen✉

In this study, we deposited $Ti_3C_2T_x$-modified, rare-earth-doped PbO_2 on the surface of a carbon fabric via electrodeposition. The surface morphology and electronic structure of the electrode were characterized with SEM, XRD and XPS. The layered $Ti_3C_2T_x$ did not change the structure of β-PbO_2, and at the same time, it improved the crystallinity of the material and reduced the grains of PbO_2. Electrochemical experiments showed that the addition of $Ti_3C_2T_x$ increased the electrochemical activity of the electrode and produced more H_2O_2, which contributed to the degradation of pollutants. The efficiency of sulfamethoxazole (SMX) degradation reached 95% after 120 min at pH 3 with a current density of 50 mA/cm^2. Moreover, the electrode has good cycling performance, and the degradation efficiency was still 80% after 120 min after 10 cycles of recycling. Based on the intermediates identified by HPLC–MS, a mechanism for SMX degradation was proposed. Our results will provide a new idea for the development of efficient electrocatalytic degradation of antibiotics.

Antibiotics are primarily used to treat diseases associated with infections in humans and animals[1–4]. Current treatment methods do not remove antibiotics effectively and pose significant risks to aquatic ecosystems and human health. Sulfonamides are common antibiotics used in aquatic environments[5]. However, the conventional activated sludge method does not degrade sulfonamide wastewater sufficiently, and the effluent quality generally fails to meet water quality standards[6]. Therefore, a water treatment technology that removes trace amounts of sulfamethoxazole (SMX) from wastewater is needed.

Electrochemical oxidation is a simple and effective method for the treatment of various organic pollutants in liquid media[7,8]. Rare earth doped PbO_2 is a promising cathode material for electrochemical oxidations of organic pollutants. Doping with rare earth elements enabled Fenton-like reactions with H_2O_2 and Ce^{4+}/Ce^{3+}[9,10] or Eu^{3+}/Eu^{2+}[11]. The rare earth elements increased the mass transfer rate of O_2, such as Ce, which generally exists in the form of CeO_2 particles. After the conversion of Ce^{4+} to Ce^{3+}, the electrode generated oxygen vacancies and adsorbed O_2 to generate H_2O_2. However, rare earth-modified PbO_2 electrodes are generally hydrophobic and unstable[12]. In addition, hydrophobic electrodes have weak electron transfer capabilities for O_2 reduction, which affect the efficiencies of H_2O_2 generation. This all affects the activities of rare-earth doped PbO_2 electrodes, and further modification is needed for improved electrochemical activity.

$Ti_3C_2T_x$, a new 2D material, was first discovered in 2011[13]. Compared with other two-dimensional materials, $Ti_3C_2T_x$ has been widely used in Electrocatalytic applications due to its thin atomic layer, high electrical conductivity, high hydrophilicity, many active sites, and good mechanical properties.[14–19]. $Ti_3C_2T_x$ increases the efficiencies of oxidation reactions and the electrochemical oxidation activity, which is essential for the production of H_2O_2[20,21]. Additionally, $Ti_3C_2T_x$ increases the efficiency of H_2O_2 decomposition: (1) Ti^{3+} and Ti^{2+} lose electrons to form Ti^{4+} and produce oxidized material[22]; (2) Most of the functional groups are hydrophilic, which facilitates the activation of H_2O_2. Doping with $Ti_3C_2T_x$ increases the conductivity of the electrode, thus reducing energy consumption[20]. In addition, the surface functional groups of 2D $Ti_3C_2T_x$ adsorb organic pollutants through electrostatic interactions, hydrogen bonding, surface complexation, and π-π interactions[23,24]. This increases the rate of antibiotic diffusion. Therefore, $Ti_3C_2T_x$ is an ideal material for electrode modification.

Therefore, we propose an innovative approach to fabricate an electrode material with a composite-structured electrode by compositing $Ti_3C_2T_x$ with a rare-earth-modified PbO_2 electrode. Based on an earlier report, we believe that by introducing $Ti_3C_2T_x$, the ability of the PbO_2 electrode to generate H_2O_2 can be effectively

Key Laboratory of Pollution Exposure and Health Intervention of Zhejiang Province, College of Biology and Environmental Engineering, Zhejiang Shuren University, Hangzhou 310015, China. ✉email: shenchaozju@163.com

enhanced, thereby improving the electrode's activity for electrocatalytic degradation of antibiotics. In this study, we used carbon fabric (CF) as the substrate. The Eu-doped PbO_2-CeO_2-Ti_3C_2@CF anode material was prepared by electrochemical deposition. Ti_3C_2 was introduced into an electrochemical conservation system. The results showed that the concentration of hydrogen peroxide generated with the Ti_3C_2 anode was three times that of the anode without Ti_3C_2. Under certain conditions, the efficiency of sulfamethoxazole degradation reached 91% in 60 min, and the anode was recycled at least ten times.

Methods

Chemicals and materials

MAX (Ti_3AlC_2) powder (90%) was purchased from Xfnano Materials Tech Co., Ltd.; hydrofluoric acid (HF, 40%) and methanol (MeOH, 99.7%) was purchased from Sinopharm Chemical Reagent Co., Ltd.; dimethyl sulfoxide (DMSO, 99.7%), $Pb(NO)_3$ (99%), and HNO_3 (65–68%) were purchased from Lingfeng Chemical Reagent Co.; $Eu(NO)_3$ (99.99%), CeO_2 (99.95%), SMX (98%) was purchased from Shanghai Aladdin Biochemical Technology Co., Ltd.; and CF was purchased from Suzhou Zhengtairong New Material Co., Ltd.

Preparation of $Ti_3C_2T_x$

Multilayered Ti_3C_2 was prepared by HF etching[25]. Then, 200 mg of Ti_3C_2 was added to 20 mL of DMSO and stirred for 24 h at room temperature. Ti_3C_2 was separated by centrifugation and dried under vacuum at 90 °C for 24 h to obtain DMSO-intercalated Ti_3C_2. After drying, 50 mL of deionized water was added and sonicated for 2 h to obtain an aqueous $Ti_3C_2T_x$ suspension.

Preparation of Eu-doped PbO_2-CeO_2-Ti_3C_2@CF

The CF was cut into 2 × 2 cm pieces and cleaned by ultrasonication with nitric acid, ethanol and deionized water in turn for 15 min. First, 0.02 mol of $Pb(NO_3)_3$, 0.04 mol of $Eu(NO_3)_3$, 0.01 mol of HNO_3 and 400 mg of CeO_2 were added to 50 ml of the previously prepared $Ti_3C_2T_x$ suspension, and deionized water was added to raise the total volume of the electrolyte 100 ml. The electrolyte was ultrasonically mixed for 30 min and then electrodeposited at a current intensity of 10 mA/cm^2 for 40 min to prepare Eu-doped PbO_2-CeO_2-Ti_3C_2@CF. Different electrode materials were prepared by changing the amounts of $Pb(NO_3)_3$, $Eu(NO_3)_3$, CeO_2 and $Ti_3C_2T_x$ suspensions.

Characterization

The surface structures of the electrodes were characterized with a Hitachi SU-70 scanning electron microscope (SEM), and the elemental distribution of the electrodes was characterized with a Bruker super-X energy dispersive X-ray spectrometer (EDS). X-ray diffraction (XRD) was performed with a Rigaku SmartLab SE diffractometer to analyze the crystal structures of the electrodes. X-ray photoelectron spectroscopy (XPS) was performed with a Thermo Scientific K-Alpha instrument and monochromatic Al Kα radiation to analyze the elemental composition, chemical state and molecular structure of the electrode surface.

Cyclic voltammetry (CV) and linear scanning voltammetry (LSV) were performed with an electrochemical workstation and a three-electrode system (CHI 760E, Shanghai Chenhua Instruments Co., Ltd., China). Eu-PbO_2-CeO_2@CF or Eu-PbO_2-CeO_2-Ti_3C_2@CF were used as the working electrodes, Pt sheets as the counter electrodes, and saturated mercuric glycol electrodes as the reference electrodes. The electrode was tested in a 0.05 M sodium sulfate solution at pH 3. CV was performed in the voltage range − 0.8 to 1 V with a sweep rate of 10 mV/s. LSV was performed in the voltage range − 1.2 to 0 V with a sweep rate of 10 mV/s.

Electrolysis

Electrolysis was conducted with a galvanostat to investigate the electrochemical performance of Eu-PbO_2-CeO_2-Ti_3C_2@CF. The antibiotics were electrolyzed in a 100 mL electrolytic cell with 0.05 M Na_2SO_4, the electrode prepared above served as the cathode and a platinum sheet as the anode, and the solution was electrolyzed in a 100 mL electrolytic cell with 0.05 Na_2SO_4 used as the electrolyte, the prepared electrode was used as the cathode, and the Pt sheet as the anode. A magnetic stirrer was used to stir the solution during the electrolysis. The effects of different experimental conditions (initial concentration, pH, and current intensity) on the degradation of SMX were explored. After every 20 min, a 3 ml water sample was taken, the SMX solution was scanned with an ultraviolet and visible (UV−Vis) spectrophotometer (Thermo Fisher Evolution 201) over the wavelength range 200–450 nm, and the concentration of SMX was determined from the peak at 262 nm. The concentration of H_2O_2 was analyzed by the potassium oxalate titanium method. Analyzing TOC in electrolytes by Shimadzu TOV-V CPH. Pb ion concentrations were measured by inductively coupled plasma (ICP, Agilent 720ES).

High-performance liquid chromatography−mass spectrometry (HPLC−MS)

Under the optimal reaction conditions, the solutions reacted for different periods were taken to determine the intermediate products. The method used an Agilent 1290-6465Q-TOF HPLC−MS system for the analyses. A C18 chromatographic column was used with a column temperature of 40 °C, a mobile phase of 40% acetonitrile and 60% pure water, including 1% HPLC grade acetic acid, a flow rate of 1 mL/min and a detection wavelength of 269 nm with an injection volume of 20 μL, and a full-scan acquisition. The mass spectra of the compounds were acquired in positive ion mode for m/z between 100 and 400.

Results and discussion

The surface morphologies of the Eu-PbO_2-CeO_2@CF (Fig. 1a,b) and Eu-PbO_2-CeO_2-Ti_3C_2@CF (Fig. 1c,d) electrodes were characterized with SEM. The Eu-PbO_2-CeO_2@CF particles were mainly pyramidal with rough surfaces and obvious height differences. With the introduction of Ti_3C_2, the grain sizes decreased obviously, and the surface was smoother and contained some circular polygonal nanocrystals. In addition, there were sheet-like structures on the surface of the Eu-PbO_2-CeO_2-Ti_3C_2@CF electrode, which were speculated to be Ti_3C_2 nanosheets. Compared to PbO_2 electrodes (Fig. S1a), this electrode with a complex surface morphology and small crystal sizes had a large electrochemically active surface area. The compositions of the Eu-PbO_2-CeO_2@CF (Table S1) and Eu-PbO_2-CeO_2-Ti_3C_2@CF (Fig. 1e) electrodes were characterized with EDS, and the Eu-PbO_2-CeO_2@CF electrode was composed of Eu, Pb, Ce, O and C, confirming the presence of Eu and CeO_2. The EDS analysis of Eu-PbO_2-CeO_2-Ti_3C_2@CF showed that, in addition to the above 5 elements, Ti was also observed, and the content was 2.05 at.%, which also confirmed the presence of Ti_3C_2.

The structures of the CF, Eu-PbO_2-CeO_2-Ti_3C_2@CF and Eu-PbO_2-CeO_2-Ti_3C_2@CF electrode were explored with XRD (Fig. 2). As seen from the graphs, the high intensities and narrow shapes of the diffraction peaks for both electrodes indicated that the electrodes were highly crystalline, suggesting that the modification with Ti_3C_2 did not affect the cleanliness of the PbO_2 substrate. Additionally, the XRD diffraction peaks were compared with those on standard PDF cards (α-PbO_2 and β-PbO_2). Most of the diffraction peaks for the two electrodes matched the diffraction peaks of β-PbO_2, and a few matched the diffraction peaks of α-PbO_2, indicating that the main component of the electrodes prepared by this method was β-PbO_2. The UV–Vis spectra (Fig. S2) also confirmed that the introduction of Ti_3C_2 did not change the structure of the electrode. In addition, based on the XRD spectra (Fig. S1b), the proportion of β-PbO_2 in the Eu-PbO_2-CeO_2@CF electrode was much larger than that in PbO_2-CeO_2@CF. α-PbO_2 had a higher electrochemical activity and lower stability than β-PbO_2. The grain sizes of both were calculated separately by Scheller's formula, and the grain size of added Ti_3C_2 was 10.5 nm, which was

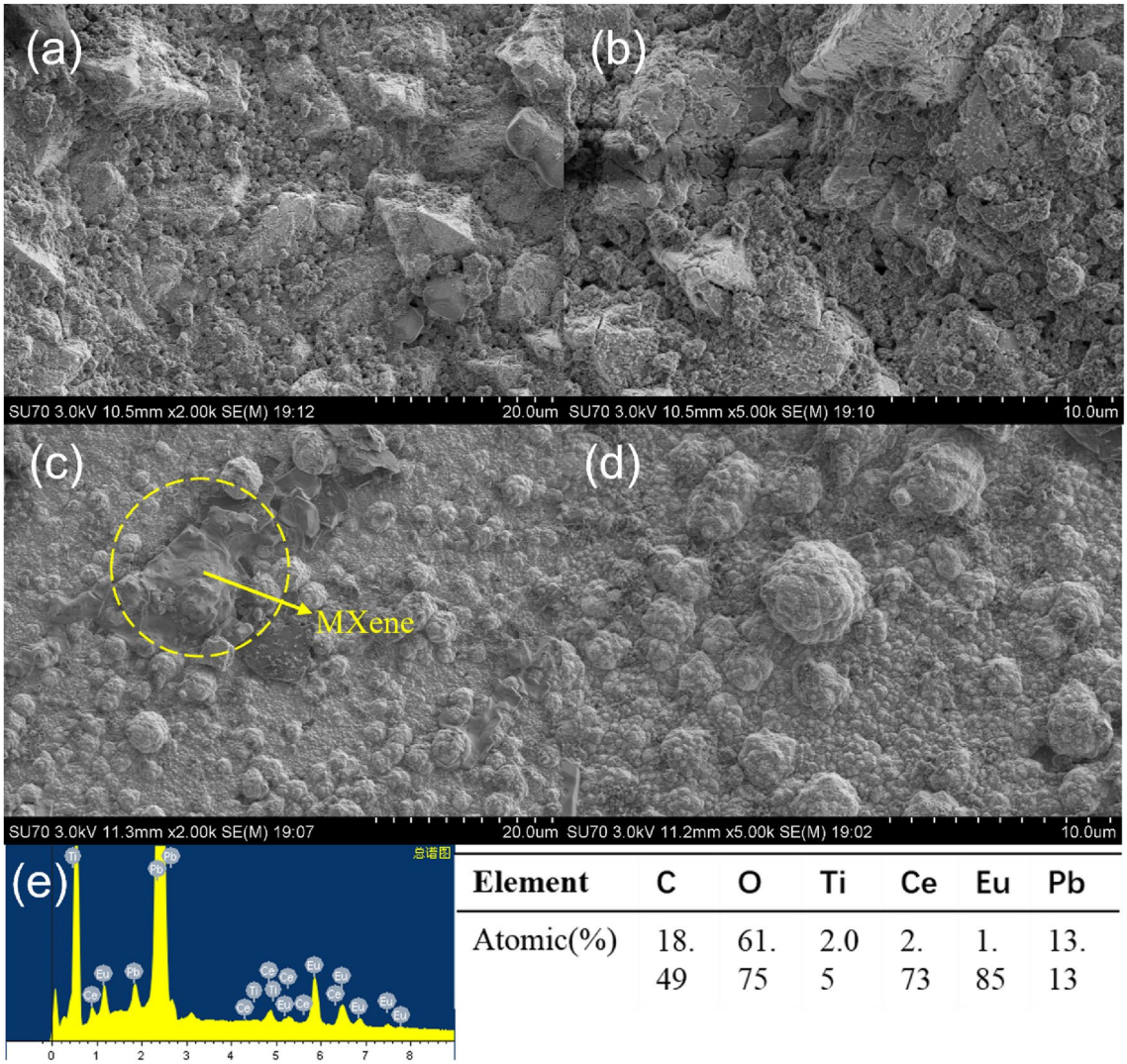

Element	C	O	Ti	Ce	Eu	Pb
Atomic(%)	18.49	61.75	2.05	2.73	1.85	13.13

Figure 1. SEM images of (**a**,**b**) Eu-doped PbO_2-CeO_2@CF and (**c**,**d**) Eu-doped PbO_2-CeO_2-Ti_3C_2@CF, (**e**) EDS spectra of Eu-doped PbO_2-CeO_2-Ti_3C_2@CF.

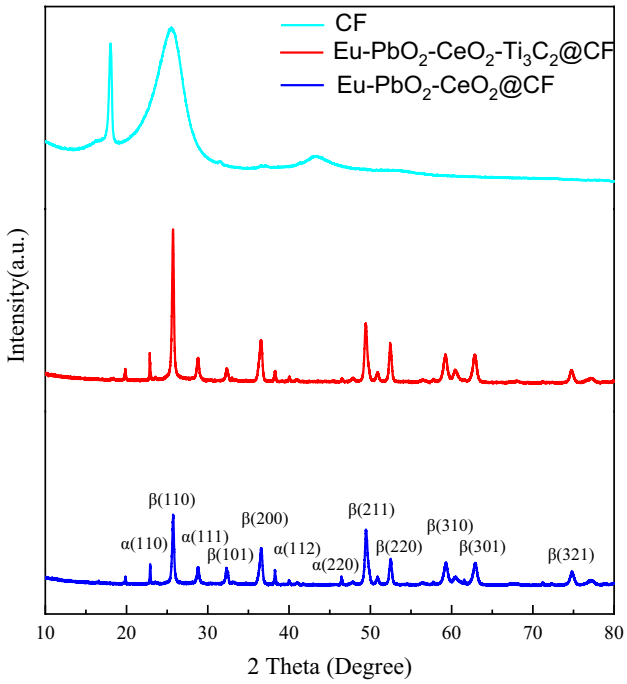

Figure 2. XRD spectra of CF, Eu-doped PbO_2-CeO2@CF and Eu-doped PbO_2-CeO_2-Ti_3C_2@CF.

much smaller than the size (28.5 nm) of unadded Ti_3C_2. The previous SEM image (Fig. 1a) also showed that the surface structure of Eu-PbO_2-CeO_2@CF was less dense and easily peeled off during the electrochemical process. In contrast, after the addition of $Ti_3C_2T_x$, the basic structure was still β-PbO_2, but the surface morphology was denser (Fig. 1c) with better stability and less likely to be peeled off.

The chemical and electronic states of Eu-PbO_2-CeO_2-Ti_3C_2@CF were analyzed by XPS (Fig. 3). During preparation of the Ti_3C_2 nanosheets, many functional groups were generated on the surface, such as OH^-, O^{2-}, and

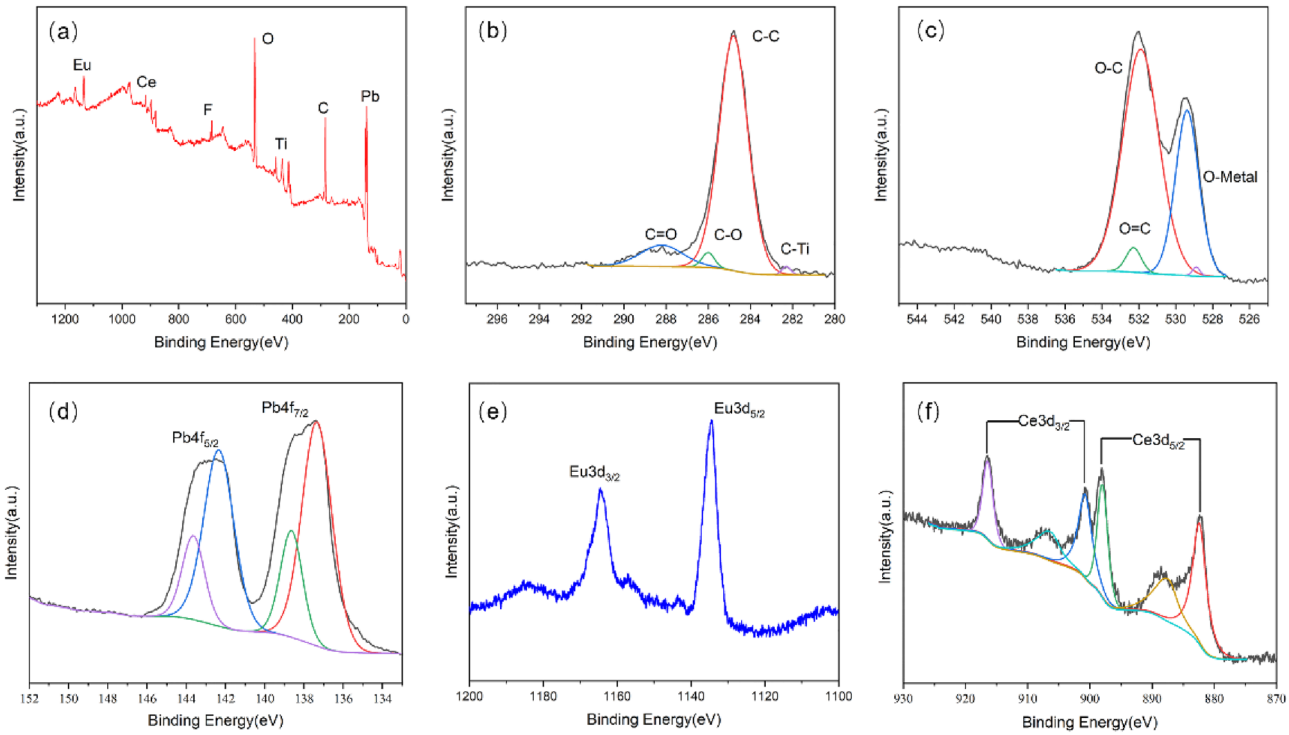

Figure 3. XPS spectra of Eu-doped PbO_2-CeO_2-Ti_3C_2@CF; (**a**) survey spectrum and (**b**) C 1s, (**c**) O 1s, (**d**) Pb 4f, (**e**) Eu 3d and (**f**) Ce 3d high resolution spectra.

F^{-}[13]. Their presence was verified by XPS (Fig. 3a). Figure 3b shows the C 1s spectrum of Eu-PbO_2-CeO_2-Ti_3C_2@CF. C-Ti bonds were present in the samples, which indicated that the Ti_3C_2 nanosheets retained their original properties after electrodeposition. The XPS spectrum of the Eu-PbO_2-CeO_2@CF electrode did not show the same peaks (Fig. S3a). Figure 3c shows the XPS spectrum of the O 1s core layer. The O 1s spectrum had three peaks at 528.8 eV, 531.9 eV and 532.3 eV associated with the Pb–O, surface O-C and O = C groups, respectively. The typical Pb 4f XPS peaks (Fig. 3d) at 137.6 eV for Eu-PbO_2-CeO_2-Ti_3C_2@CF were assigned to Pb^{4+}. The peak at 138.5 eV is the formation of a small amount of $PbCO_3$ on the surface as a result of the binding of PbO_2 to CO_2 in the air. Figure 3e,f shows the Eu 3d and Ce 3d XRD data. Ce 3d has a clear spin–orbit splitting peak and the Ce $3d_{5/2}$ peak at the rightmost 882.18 eV confirms the presence of CeO_2 nanoparticles.

The H_2O_2 generated in the electrochemical oxidation system is critical for the degradation of SMX. Therefore, the concentration of H_2O_2 was studied spectrophotometrically with potassium titanyl oxalate (Fig. 4a). The concentration of H_2O_2 increased sharply in the first 20 min, reaching a peak at 40 min. The activity of the electrode in generating H_2O_2 increased with the addition of Ti_3C_2. The electrode prepared by adding 200 mg of Ti_3C_2 to the electrolyte produced three times more H_2O_2 than the electrode without Ti_3C_2 and 1.5 times more H_2O_2 than the electrode with 100 mg of Ti_3C_2. The CV and LSV curves of the Eu-PbO_2-CeO_2@CF (black) and Eu-PbO_2-CeO_2-Ti_3C_2@CF (red) electrodes were then generated separately. As shown in Fig. 4b, the redox peak current and peak area for Eu-PbO_2-CeO_2-Ti_3C_2@CF were significantly greater than those for Eu-PbO_2-CeO_2@CF. Figure 4c shows that the PbO_2-CeO_2-Ti_3C_2@CF cathode had a stronger current response when a strong reduction peak corresponding to the ORR process was observed, as the Ti_3C_2 material significantly improved the electron transfer and catalytic activity of the ORR. Thus, when assembled into an electrochemical oxidation system, the PbO_2-CeO_2-Ti_3C_2@CF cathodes enabled in situ generation of -OH and contaminant degradation.

To determine the optimal ratio of $Pb(NO_3)_3$, $Eu(NO_3)_3$ and CeO_2, the efficiencies of SMX degradation at these electrodes were studied by varying the concentrations in the electrolyte and under established conditions (an initial SMX concentration of 30 mg/L, an initial pH of 3 and an applied current density of 50 mA/cm^2) (Fig. S4). The electrolytic efficiencies of the prepared electrodes were highest when the concentrations of $Pb(NO_3)_3$, $Eu(NO_3)_3$ and CeO_2 were 2 mol/L, 4 mol/L and 2 g/L, respectively. The rate of SMX degradation reached 85% after 2 h.

Based on these results, 2 g/L $Ti_3C_2T_x$ was added to the electrolyte, and the efficiency of SMX degradation was investigated under the same conditions (Fig. 5a). For electrodes with different Pb and Eu ratios, the addition of $Ti_3C_2T_x$ improved the rate of SMX degradation. For the electrode with a Pb: Eu ratio of 2:4, the degradation efficiency increased by 10% with the addition of $Ti_3C_2T_x$ and reached 95% at 120 min. Then the TOC in the electrolyte was detected by a TOC analyzer, and it was 4.04 mg/L, with a removal rate of 71.6%. According to the relevant literature[26–29], the concentration of SMX currently has been much smaller than the minimum inhibitory concentration. During degradation, the rate of the electrode reaction was calculated as:

$$\ln C_0/C_t = kt \quad (1)$$

where C_0 (mg/L) and C_t (mg/L) are the SMT concentrations at time 0 and t min, respectively (Fig. 5b). All four electrodes fit the first order kinetic model. With the addition of $Ti_3C_2T_x$, the electrolytic (Pb:Eu = 2:4) degradation rate constantly increased from 0.0157 ± 0.00052 to 0.0240 ± 0.0011. Moreover, the degradation rate of the electrode without $Ti_3C_2T_x$ was slower in the first 20 min compared to that of the electrode with $Ti_3C_2T_x$. This was mainly due to the reduction rate of O_2 on the hydrophobic surface and the lower efficiency of H_2O_2 activity. The addition of $Ti_3C_2T_x$ increased the hydrophilic functional groups and improved the degradation activity. The electrode degradation activity of Eu-PbO_2-CeO_2-Ti_3C_2@CF was compared with that of electrodes reported in the literature (Table 1). Eu-PbO_2-CeO_2-Ti_3C_2@CF showed excellent activity at higher initial concentrations of SMX and without additional ventilation.

To demonstrate the high electrocatalytic activity of the electrode, the effects of different operating parameters (including the initial concentration, current density and pH) on the electrochemical oxidation efficiency were investigated (Fig. 6).

Figure 6a shows the effect of initial SMX concentrations on SMX degradation efficiency. The experimental conditions included a current density of 50 mA/cm^2, a pH of 3 and SMX concentrations of 10, 30 and 50 mg/L. As the concentration of the pollutant decreased, the degradation efficiency of SMX increased, but the amount of degradation decreased. This was mainly because at low concentrations, electrocatalytic oxidation was faster

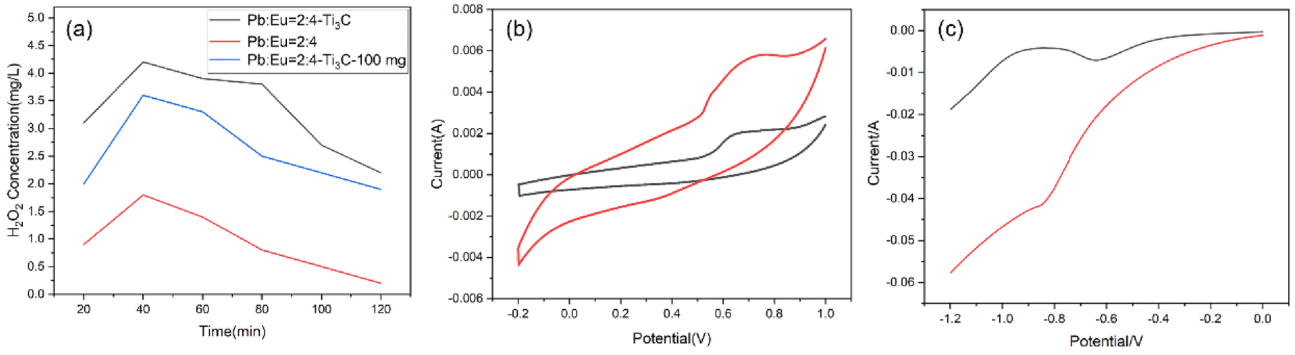

Figure 4. (**a**) Evolution of the H_2O_2 concentration, (**b**) CV data, and (**c**) LSV data for Eu-doped PbO_2-CeO_2@CF (black) and Eu-doped PbO_2-CeO_2-Ti_3C_2@CF (red).

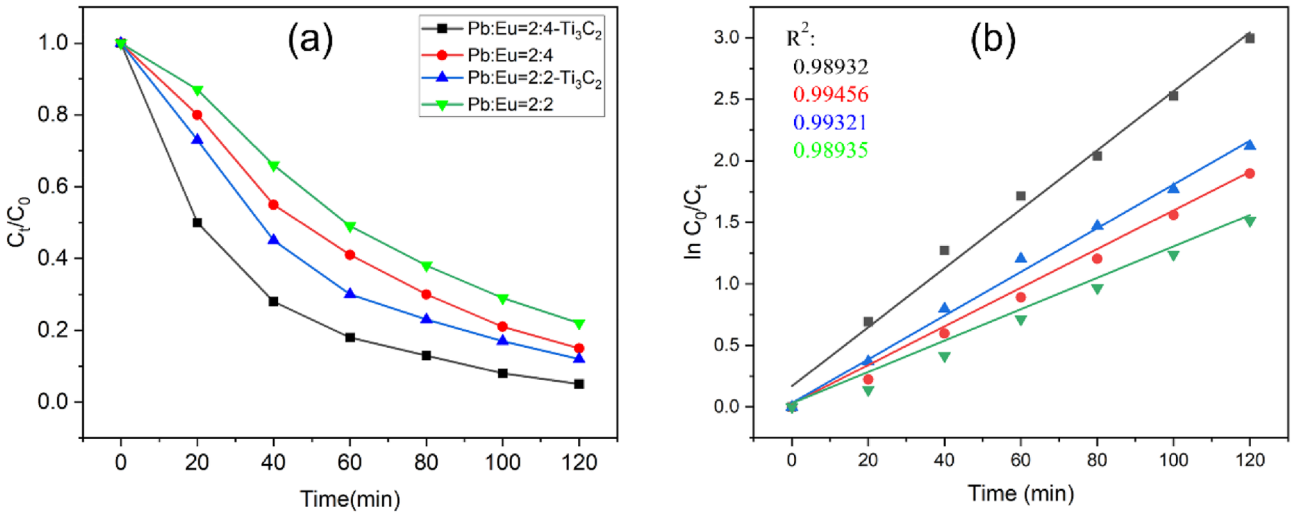

Figure 5. (**a**) SMX degradation with Eu-doped PbO_2-CeO_2@CF and Eu-doped PbO_2-CeO_2-Ti_3C_2@CF and (**b**) kinetic analyses with the pseudo-first-order model.

Entry	Electrodes	Degradation Condition	Removal efficiency (%)	References
1	Eu-doped PbO_2-CeO_2-Ti_3C_2@CF	30 mg/L, pH: 3 50 mA/cm^2	95	This work
2	$Mn_{0.67}Fe_{0.33}$-MOF-74@CF	10 mg/L, pH: 3 30 mA/ cm^2 Continuously ventilated	96	Ref.[2]
3	Nb/BDD	10 mg/L 2.5 A Oxygen injection	95	Ref.[5]
4	GAC@Ni/Fe	1 mg/L 5 V Continuously ventilated	90.8	Ref.[43]

Table 1. Comparison of Eu-doped PbO_2-CeO_2-Ti_3C_2@CF with some recently reported electrodes for SMX degradation.

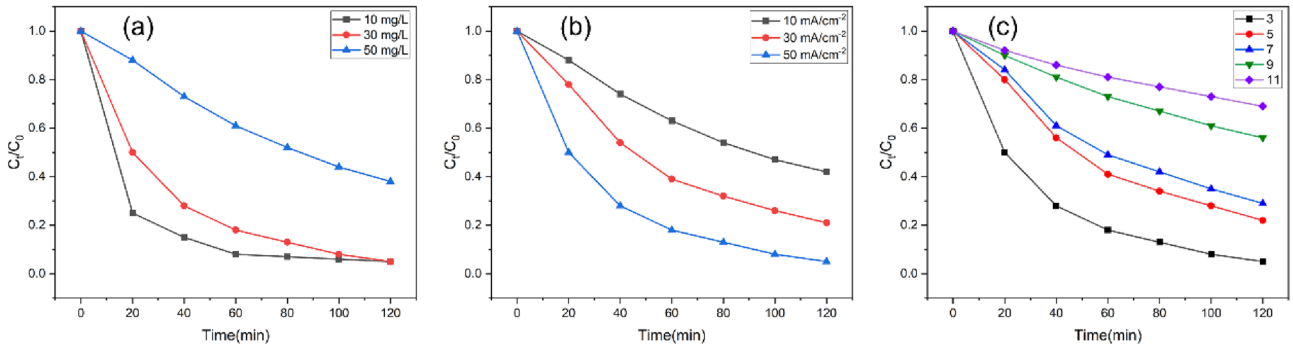

Figure 6. Effects of (**a**) SMX initial concentration, (**b**) current density, and (**c**) initial pH of the solution on the removal of SMX by the Eu-doped PbO_2-CeO_2-Ti_3C_2@CF electrode.

than diffusion, thus allowing effective degradation of the organic matter. As the concentration of the pollutant increased, so did the amount of organic matter produced during degradation, including pollutants and intermediate products. In addition, the electrode produced a limited number of hydroxyl radicals. As the pollutant concentration increased, the number of hydroxyl radicals acting per unit of pollutant decreased, which made the degradation of SMX less effective[30]. Therefore, an SMX concentration of 30 mg/L was chosen for subsequent experiments.

The current density is a key factor in the electrochemical oxidation process because it regulates the generation of hydroxyl radicals[31]. Figure 6b shows the rate of SMX removal for different applied current densities. As the current density was increased from 10 to 50 mA/cm^2, the efficiency of SMX removal increased from 58 to 95%. When the current density was increased from 30 to 50 mA/cm^2, the increase in the degradation efficiency

was smaller than before. The higher current density may have enhanced the reaction of oxygen on the anode surface, thus competing with the oxidation of organic matter on the electrodes surface and affecting the removal efficiency[32]. In addition, the diffusion rate of contaminants to the electrode is limited at the same concentration, limiting the degradation rate at high currents and decreasing the current efficiency. Therefore, after careful consideration, the SMX degradations were performed at a current density of 50 mA/cm^2.

Figure 6c shows the effect of different pHs on the efficiency of SMX degradation[33]. The results show that the fastest SMX degradation rate was achieved at pH 3. This is because hydroxyl radicals are more favorable for SMX degradation under acidic conditions[34]. In addition, CO_2 was the main product from electrochemical degradation of SMX, and under alkaline conditions, CO_2 dissolved in the solution and inhibited pollutant oxidation. Based on the above analysis, pH 3 was used as the initial pH for the electrochemical degradation of SMX.

The cycling performance of the electrodes was investigated. The SMX cycled for 120 min under the optimal conditions for SMX degradation. After each run, the degradation rate of SMX decreased slightly and remained at 80% after 10 cycles (Fig. 7). In addition, the electrodes after electrochemical degradation were characterized by XRD (Fig. S5), it can be found that the structure as well as the morphology did not change significantly. In addition, the content of Pb ions in the electrolyte was detected by ICP-MS, and the concentration of Pb ion released from the Eu-PbO_2-CeO_2-Ti_3C_2@CF electrode was 3.68 μg/L, which is less than the World Health Organization's requirements for lead ion concentrations in drinking water and China's permitted effluent discharge standards for Pb in surface waters. Therefore, the electrochemical degradation of this electrode is safe and reliable for the environment and human health. Therefore, the Eu-PbO_2-CeO_2-Ti_3C_2@CF electrode had good stability.

To further investigate the mechanism of SMX degradation, methanol was used as a scavenger (Fig. S6) to investigate the role of ·OH. It can be found that the degradation efficiency of SMX decreased significantly after the addition of methanol, indicating that ·OH plays a major role in the degradation process.

To further investigate the degradation mechanism, The intermediates produced during SMX degradation were characterized by HPLC–MS (Table S2). Possible degradation pathways have been proposed in conjunction with the literature (Fig. 8).

In pathway I, the degradation pathway was hydroxylation of the arene ring. The aniline portion was attacked by the hydroxyl radical, resulting in the disappearance of the amine group and the formation of 255[35].

In pathway II, the amino group on the arene ring in SMX was attacked by a hydroxyl radical to form NO_2-SMX (283)[36]. Subsequently, the S—N bond of NO_2-SMX was cleaved to give 155 and 99[37]. In addition, ·OH react with the isoxazole ring to form 288[38]. Subsequently, the C-N bond breaks and 158 and 132 are formed. Then, 158 lost a -NH_2 to form 141. Ions 132 and 99 coupled with N-centered radicals to form 227[39]. The remaining 99 was stripped of a methyl group to form 85[40].

In pathway 3, the isoxazole ring in SMX opened to form 256, followed by C-N bond breakage to form 174[41]. Subsequent coupling was centered around the N atom to form 340[42]. All intermediates eventually degrade to water, carbon dioxide and inorganic ions.

Conclusion

In summary, $Ti_3C_2T_x$-modified rare earth element-doped PbO_2 electrodes were prepared via electrodeposition and were fully characterized by SEM, XRD, and XPS. The results showed that $Ti_3C_2T_x$ was doped into the PbO_2 electrode and optimized the surface morphology as well as the electronic structure of the electrode. The optimal degradation conditions for the electrochemical degradation of SMX by electrodes were also investigated. The

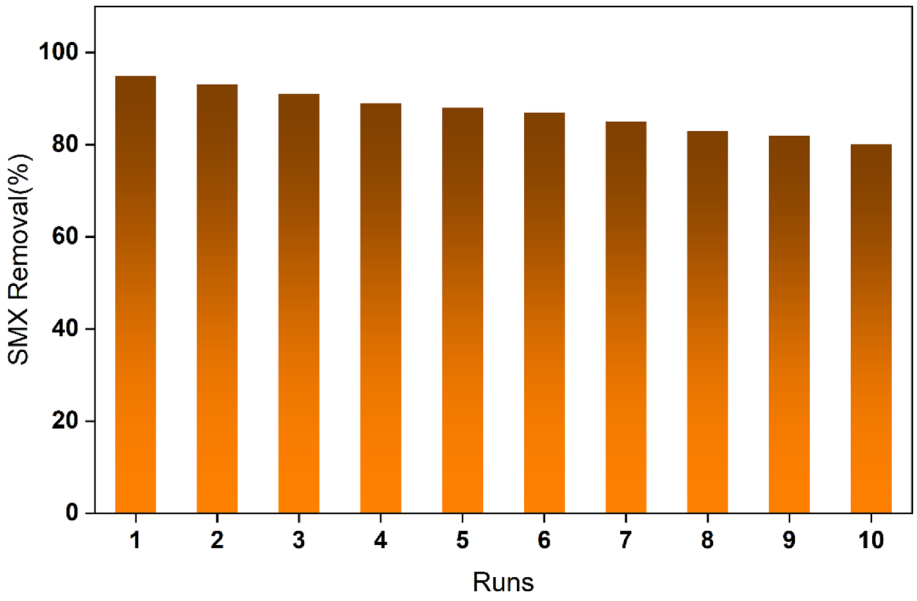

Figure 7. Recycling and reuse of the Eu-doped PbO_2-CeO_2-Ti_3C_2@CF electrode.

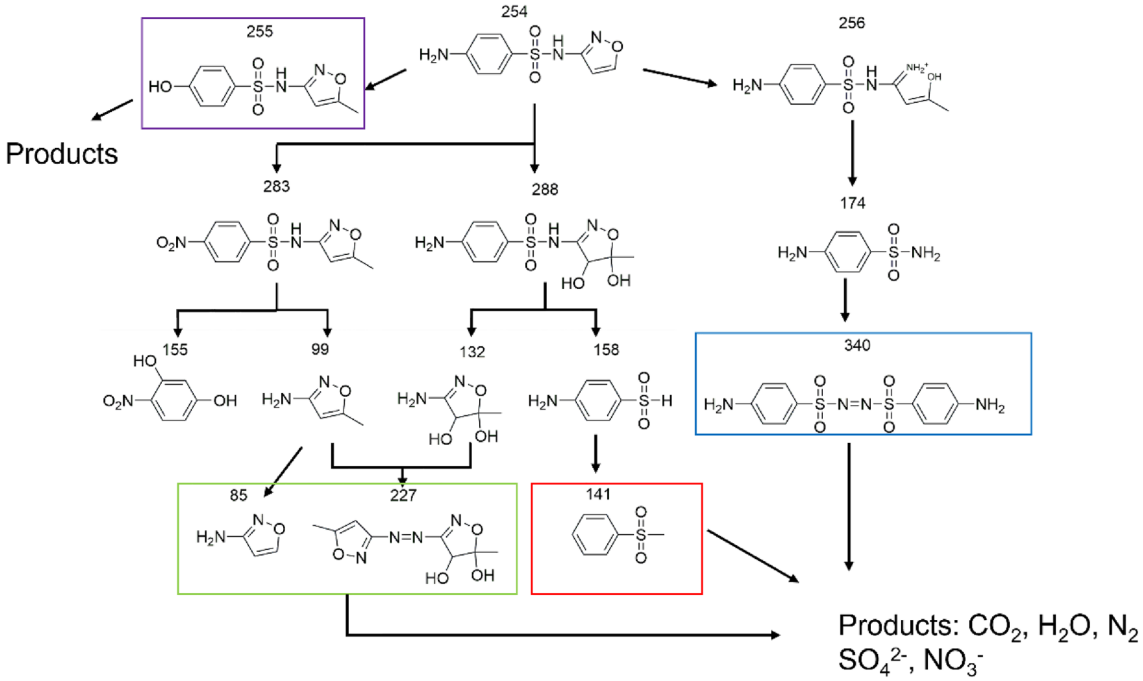

Figure 8. Degradation pathways for SMX.

electrodes showed good stability and were recycled and reused at least 10 times. In addition, a degradation pathway was proposed based on an analysis of the HPLC–MS intermediates. All these results indicate that $Ti_3C_2T_x$ is an ideal electrochemical oxidation modification material, which can effectively improve the electrochemical activity of the electrode. This work provides a new idea for electrode modification, which has a broad and great application prospect in treating difficult-to-degrade medical wastewater.

Data availability

The datasets used and/or analyzed during the current study available from the corresponding author on reasonable request.

Received: 25 January 2024; Accepted: 4 April 2024
Published online: 05 April 2024

References

1. Zhao, Z. *et al.* Investigation of the degradation and dehalogenation properties of florfenicol by heterogeneous Fenton reaction activated with MIL-53(Al)-supported nano zero-valent iron. *Chem. Eng. J.* **453**, 139420 (2023).
2. Wu, D. *et al.* Two-dimensional manganese-iron bimetallic MOF-74 for electro-Fenton degradation of sulfamethoxazole. *Chemosphere* **327**, 138514 (2023).
3. Xu, W., Zheng, X., Shangguan, Z., Qu, J. & Zhang, W. A low-cost magnetic catalyst ($MnFe_2O_4$) for ciprofloxacin degradation via periodate activation: The synergistic effect of Mn and Fe. *Chem. Eng. J.* **464**, 142562 (2023).
4. Shen, J. *et al.* Visible light-mediated ring opening and cyclization of aryl cyclopropanes: Efficient synthesis of pyrrolo[1,2- *a*] quinoxalin-4(5 *H*)-ones with antineoplastic activity. *Org. Chem. Front.* **11**, 1758–1764 (2024).
5. García-Espinoza, J. D. & Nacheva, P. M. Degradation of pharmaceutical compounds in water by oxygenated electrochemical oxidation: Parametric optimization, kinetic studies and toxicity assessment. *Sci. Total. Environ.* **691**, 417–429 (2019).
6. Song, Y. *et al.* Photodegradation of sulfonamides by g-C_3N_4 under visible light irradiation: Effectiveness, mechanism and pathways. *Appl. Catal. B-environ.* **210**, 88–96 (2017).
7. Qi, H., Shi, X., Liu, Z., Yan, Z. & Sun, Z. In situ etched graphite felt modified with $CuFe_2O_4$/Cu_2O/Cu catalyst derived from CuFe PBA for the efficient removal of sulfamethoxazole through a heterogeneous electro-Fenton process. *Appl. Catal. B-environ.* **331**, 122722 (2023).
8. Miao, L. *et al.* Norfloxacin degradation in synthetic human urine using nickel converter slag-laterite heterogeneous Electro-Fenton process. *J. Water Process. Eng.* **53**, 103723 (2023).
9. Song, Y., Wei, G. & Xiong, R. Structure and properties of PbO_2–CeO_2 anodes on stainless steel. *Electrochim. Acta.* **52**, 7022–7027 (2007).
10. Yao, Y. *et al.* Preparation and characterization of PbO_2 -CeO_2 nanocomposite electrode with high cerium content and its appplication in the electrocatalytic degradation of malachite green. *J. Electrochem. Soc.* **162**, H693–H698 (2015).
11. Zhang, Z. *et al.* Electrochemical oxidation of hydroquinone using Eu-doped PbO_2 electrodes: Electrode characterization, influencing factors and degradation pathways. *J. Electroanal. Chem.* **895**, 115493 (2021).
12. Lyu, J. *et al.* Enhancement of the electrocatalytic oxidation of dyeing wastewater (reactive brilliant blue KN-R) over the Ce-modified Ti-PbO_2 electrode with surface hydrophobicity. *J. Solid State Electr.* **23**, 847–859 (2019).
13. Naguib, M. *et al.* Two-dimensional nanocrystals produced by exfoliation of Ti_3AlC_2. *Adv. Mater.* **23**, 4248–4253 (2011).
14. Zhu, J. *et al.* Recent advance in MXenes: A promising 2D material for catalysis, sensor and chemical adsorption. *Coord. Chem. Rev.* **352**, 306–327 (2017).
15. Ma, X. *et al.* Degradable $Ti_3C_2T_x$ MXene nanosheets containing a lignin polyurethane photothermal foam (LPUF) for rapid crude oil cleanup. *ACS Appl. Nano Mater.* **5**, 2848–2858 (2022).

16. Li, W. *et al.* Peroxymonosulfate activation by oxygen vacancies-enriched MXene nano-Co_3O_4 co-catalyst for efficient degradation of refractory organic matter: Efficiency, mechanism, and stability. *J. Hazard. Mater.* **432**, 128719 (2022).
17. Li, Y. *et al.* 1T-MoS_2 nanopatch/Ti_3C_2 MXene/TiO_2 nanosheet hybrids for efficient photocatalytic hydrogen evolution. *Mater. Chem. Front.* **3**, 2673–2680 (2019).
18. Kannan, K. *et al.* Two dimensional MAX supported copper oxide/nickel Oxide/MAX as an efficient and novel photocatalyst for hydrogen evolution. *Int. J. Hydrogen Energ.* **48**, 7273–7283 (2023).
19. Chanda, D. *et al.* Effect of the interfacial electronic coupling of nickel-iron sulfide nanosheets with layer Ti_3C_2 MXenes as efficient bifunctional electrocatalysts for anion-exchange membrane water electrolysis. *Appl. Catal. B-Environ.* **321**, 122039 (2023).
20. Ma, Y., Lv, X., Xiong, D., Zhao, X. & Zhang, Z. Catalytic degradation of ranitidine using novel magnetic Ti_3C_2-based MXene nanosheets modified with nanoscale zero-valent iron particles. *Appl. Catal. B-Environ.* **284**, 119720 (2021).
21. Xia, Y. *et al.* Fabrication of novel FeS_2 NWs/Ti_3C_2 cathode for Photo-Electro-Fenton degradation of sulfamethazine. *Chem. Eng. J.* **426**, 130719 (2021).
22. Yang, P. *et al.* Singlet oxygen-dominated activation of peroxymonosulfate by CuO/MXene nanocomposites for efficient decontamination of carbamazepine under high salinity conditions: Performance and singlet oxygen evolution mechanism. *Sep. Purif. Technol.* **285**, 120288 (2022).
23. Sun, X., Yang, J., Su, D., Wang, C. & Wang, G. Highly efficient adsorption of bilirubin by $Ti_3C_2T_x$ MXene. *Chem-Asian J.* **16**, 1949–1955 (2021).
24. Ghani, A. A. *et al.* Adsorption and electrochemical regeneration of intercalated $Ti_3C_2T_x$ MXene for the removal of ciprofloxacin from wastewater. *Chem. Eng. J.* **421**, 127780 (2021).
25. Zhu, D. *et al.* One-step synthesis of PdCu@Ti_3C_2 with high catalytic activity in the Suzuki-Miyaura coupling reaction. *Nanoscale Adv.* **4**, 3362–3369 (2022).
26. Baskin, H., Dogan, Y., Bahar, I. H. & Yulug, N. Effect of subminimal inhibitory concentrations of gentamicin, penicillin, trimethoprim-sulfamethoxazole on adherence of uropathogenic Escherichia coli strains. *J. Chemother.* **14**, 161–165 (2002).
27. Ho, M.-C. *et al.* Antimicrobial susceptibility, inimum inhibitory concentrations, and clinical profiles of stenotrophomonas maltophilia endophthalmitis. *Microorganisms* **9**, 1840 (2021).
28. Voigt, M., Bartels, I., Nickisch-Hartfiel, A. & Jaeger, M. Determination of minimum inhibitory concentration and half maximal inhibitory concentration of antibiotics and their degradation products to assess the eco-toxicological potential. *Toxicol Environ. Chem.* **101**, 315–338 (2019).
29. Ho, M.M.-C. *et al.* Antibiotic Susceptibility and minimum inhibitory concentration for stenotrophomonas maltophilia ocular infections. *Antibiotics* **11**, 1457 (2022).
30. Dolatabadi, M. *et al.* Simultaneous electrochemical degradation of pesticides from the aqueous environment using Ti/SnO_2–Sb_2O_3/PbO_2/Bi electrode; process modeling and mechanism insight. *Chemosphere* **311**, 137001 (2023).
31. Chen, J., Xia, Y. & Dai, Q. Electrochemical degradation of chloramphenicol with a novel Al doped PbO_2 electrode: Performance, kinetics and degradation mechanism. *Electrochim. Acta.* **165**, 277–287 (2015).
32. Phan Quang, H. H. *et al.* Advanced electro-Fenton degradation of a mixture of pharmaceutical and steel industrial wastewater by pallet-activated-carbon using three-dimensional electrode reactor. *Chemosphere* **297**, 134074 (2022).
33. Dolatabadi, M., Świergosz, T., Wang, C. & Ahmadzadeh, S. Accelerated degradation of groundwater-containing malathion using persulfate activated magnetic Fe_3O_4/graphene oxide nanocomposite for advanced water treatment. *Arab. J. Chem.* **16**, 104424 (2023).
34. Rosales, E., Pazos, M. & Sanromán, M. A. Advances in the electro-Fenton process for remediation of recalcitrant organic compounds. *Chem. Eng. Technol.* **35**, 609–617 (2012).
35. Hai, H., Xing, X., Li, S., Xia, S. & Xia, J. Electrochemical oxidation of sulfamethoxazole in BDD anode system: Degradation kinetics, mechanisms and toxicity evaluation. *Sci. Total Environ.* **738**, 139909 (2020).
36. Yu, Y., Ji, Y., Lu, J., Yin, X. & Zhou, Q. Degradation of sulfamethoxazole by Co_3O_4-palygorskite composites activated peroxymonosulfate oxidation. *Chem. Eng. J.* **406**, 126759 (2021).
37. Wang, W. *et al.* Kapok fiber derived biochar as an efficient electro-catalyst for H_2O_2 in-situ generation in an electro-Fenton system for sulfamethoxazole degradation. *J. Water Process. Eng.* **50**, 103311 (2022).
38. Hu, Z.-T. *et al.* Enhanced $BiFeO_3$/$Bi_2Fe_4O_9$/H_2O_2 heterogeneous system for sulfamethoxazole decontamination: system optimization and degradation pathways. *J. Colloid Interf. Sci.* **577**, 54–65 (2020).
39. Du, J., Guo, W., Che, D. & Ren, N. Weak magnetic field for enhanced oxidation of sulfamethoxazole by Fe0/H_{2O}2 and Fe0/persulfate: performance, mechanisms, and degradation pathways. *Chem. Eng. J.* **351**, 532–539 (2018).
40. Zhao, G., Li, W., Zhang, H., Wang, W. & Ren, Y. Single atom Fe-dispersed graphitic carbon nitride (g-C_3N_4) as a highly efficient peroxymonosulfate photocatalytic activator for sulfamethoxazole degradation. *Chem. Eng. J.* **430**, 132937 (2022).
41. Qi, H., Sun, X. & Sun, Z. Cu-doped Fe_2O_3 nanoparticles/etched graphite felt as bifunctional cathode for efficient degradation of sulfamethoxazole in the heterogeneous electro-Fenton process. *Chem. Eng. J.* **427**, 131695 (2022).
42. Guo, R. *et al.* Efficient degradation of sulfamethoxazole by CoCu LDH composite membrane activating peroxymonosulfate with decreased metal ion leaching. *Chem. Eng. J.* **417**, 127887 (2021).
43. Li, S., Lin, Y., Zhu, S. & Liu, G. Electrocatalytic degradation of sulfamethylthiadiazole by GAC@Ni/Fe three-dimensional particle electrode. *Environ. Sci. Pollut. R.* **29**, 57112–57126 (2022).

Acknowledgements

We thank Sujuan Ding and Yichen Li from Zhejiang University for the SEM measurements. The authors would like to thank Zhiqi Liu and Qiannan Ma from Shiyanjia Lab (www.shiyanjia.com) for XRD, and XPS analyses.

Author contributions

C.S. and D.Z. conceived the project; D.Z. and Y.W. carried out most of the experiments and analyzed the data with the assistance of K.Z. and H.X. C.C. and J.Q. contributed to the discussions; D.Z. and C.S. co-wrote the paper with the inputs and suggestions from others.

Funding

Financial support was provided by the National Natural Science Foundation of China (No. 22302178) and Zhejiang Provincial Natural Science Foundation of China (Grant No. LQ21E020003).

Competing interests

The authors declare no competing interests.

Additional information

Supplementary Information The online version contains supplementary material available at https://doi.org/10.1038/s41598-024-58893-z.

Correspondence and requests for materials should be addressed to C.S.

Reprints and permissions information is available at www.nature.com/reprints.

Publisher's note Springer Nature remains neutral with regard to jurisdictional claims in published maps and institutional affiliations.